Formation, Characterization, and Sub-50-nm Patterning of Organosilane Monolayers with Embedded Disulfide Bonds: An Engineered Self-Assembled Monolayer Resist for Electron-Beam Lithography

Xuejun Wang,† Wenchuang Hu,‡ Rajagopal Ramasubramaniam,‡ Gary H. Bernstein,‡ Gregory Snider,‡ and Marya Lieberman*,†

Department of Chemistry and Biochemistry and Department of Electrical Engineering, University of Notre Dame, Notre Dame, Indiana 46556

Received July 16, 2003. In Final Form: August 23, 2003

This paper describes self-assembled monolayers (SAMs) that contain embedded disulfide bonds and the selective cleavage of the disulfides by electron-beam lithography (EBL). Phenyl(3-trimethoxysilylpropyl)-disulfide (**I**) forms siloxane SAMs with a root-mean-square roughness of 1.8 Å. The disulfide bonds in **I** remain intact in the SAM and can react with dithiothreitol after monolayer formation, forming surface thiols, which can be derivatized with maleimide dyes. Atomic force microscopy (AFM) anodization and EBL have been used to create high-resolution patterns on the disulfide-containing monolayer. AFM anodization on monolayer **I** achieves 20-nm resolution lines with both topographic and chemical alterations in the patterned region. EBL with an accelerating voltage of 30 kV generates trenches 3−4 Å deep and 30 nm wide. According to AFM topographic and friction images, X-ray photoelectron spectroscopy damage simulation, and chemical rebinding tests, the chemical changes induced by EBL are consistent with cleavage of the disulfide bonds to form sulfhydryl groups. The resulting chemical patterns can be further developed by reaction with *N*-(1-pyrene)maleimide.

Introduction

The patterning of ultrathin self-assembled monolayers (SAMs) has attracted tremendous attention, because of the potential applications in various fields such as sensor design, DNA chips,[1] resists,[2] molecular electronics,[3] microelectronics, and electrochemistry. Micrometer-sized patterns have been generated on SAMs, using techniques such as ultraviolet (UV) lithography,[4] deep-UV lithography[5] and microcontact printing (μCP).[6] Nanoscale patterning of SAMs has been achieved by electron-beam lithography (EBL)[7] and scanning probe lithography.[8] Recently, several nanoscale, chemically selective patterning processes have been reported. For instance, Gölzhäuser et al. reported the selective conversion of terminal nitro groups of organothiol monolayers on gold with low-energy electron beams.[9] Maoz et al. described spatially defined electro-oxidation of terminal groups of alkylsilane SAMs on Si surfaces.[10] Both groups of researchers demonstrated that such patterned monolayers can be used as templates for the site-selective immobilization of molecules.[11,12]

Design of a Self-Assembled Monolayer Engineered for High-Resolution Patterning

The phenyl(3-trimethoxysilylpropyl)disulfide molecule (**I**) was designed to form well-ordered SAMs with an internal disulfide bond. Disulfide bonds are easy to synthesize, moderately reactive, and not too bulky. By analogy to known solution reactivity, embedded disulfide bonds could be cleaved, cross-linked, or otherwise modified by EBL or atomic force microscopy (AFM) anodization to yield nanoscale patterns. Cleavage of the internal (as opposed to terminal) functional groups in a SAM would cause topographic change, as well as chemical change, which would be useful for optimization of the patterning process. The functional groups that are formed by various reactions of disulfides are chemically quite different from the hydrocarbon matrix of the SAM; therefore, the chemical changes caused by EBL or AFM anodization could be used to define where other molecules or nanoparticles bind to the surface.

Disulfide bonds are relatively weak (they have a bond energy of ∼55 kcal/mol) and can be reductively cleaved with dithiothreitol (DTT) in solution or on a surface to form thiol groups.[13] Although a chemical reductant cannot easily be delivered to a desired spatial location, an electrochemical reductant, namely electrons, can be

* Author to whom correspondence should be addressed. E-mail: mlieberm@nd.edu.
† Department of Chemistry and Biochemistry.
‡ Department of Electrical Engineering.

(1) Pirrung, M. C. *Angew Chem., Int. Ed.* **2002**, *41*, 1276−1289.
(2) Lercel, M. J.; Rooks, M.; Tiberio, R. C.; Craighead, H. G.; Sheen, C. W.; Parikh, A. N.; Allara, D. L. *J. Vac. Sci. Technol. B* **1995**, *13*, 1139−1143.
(3) Reed, M. A.; Tour, J. M. *Sci. Am.* **2000**, *282*, 86−93.
(4) (a) Tarlov, M. J.; Burgess, D. R. F.; Gillen, G. *J. Am. Chem. Soc.* **1993**, *115*, 5303−5306. (b) Huang, J. Y.; Dahlgren, D. A.; Hemminger, J. C. *Langmuir* **1994**, *10*, 626−628.
(5) Dulcey, C. S.; Georger, J. H., Jr.; Krauthamer, V.; Stenger, D. A.; Fare, T. L.; Calvert, J. M. *Science* **1991**, *252*, 551−554.
(6) Kumar, A.; Abbott, N. L.; Kim, E.; Biebuyck, H. A.; Whitesides, G. M. *Acc. Chem. Res.* **1995**, *28*, 219−226.
(7) Lercel, M. J.; Craighead, H. G.; Parikh, A. N.; Seshadri, K.; Allara, D. L. *Appl. Phys. Lett.* **1996**, *68*, 1504−1506.
(8) Liu, G.-Y.; Xu, S.; Qian, Y. *Acc. Chem. Res.* **2000**, *33*, 457−466.
(9) Eck, W.; Stadler, V.; Geyer, W.; Zharnikov, M.; Golzhauser, A.; Grunze, M. *Adv. Mater.* **2000**, *12*, 805−808.
(10) Maoz, R.; Cohen, S. R.; Sagiv, J. *Adv. Mater.* **1999**, *11*, 55−61.
(11) Golzhauser, A.; Eck, W.; Geyer, W.; Stadler, V.; Weimann, T.; Hinze, P.; Grunze, M. *Adv. Mater.* **2001**, *13*, 806−809.
(12) (a) Maoz, R.; Frydman, E.; Cohen, S. R.; Sagiv, J. *Adv. Mater.* **2000**, *12*, 424−429. (b) Maoz, R.; Frydman, E.; Cohen, S. R.; Sagiv, J. *Adv. Mater.* **2000**, *12*, 725−731. (c) Hoeppener, S.; Maoz, R.; Cohen, S. R.; Chi, L.; Fuchs, H.; Sagiv, J. *Adv. Mater.* **2002**, *14*, 1036−1041.
(13) Ichinose, N.; Sugimura, J.; Uchida, T.; Shimo, N. *Chem. Lett.* **1993**, *11*, 1961.

10.1021/la035291e CCC: $25.00
Published on Web 10/10/2003

Scheme 1. Synthesis of Compound I

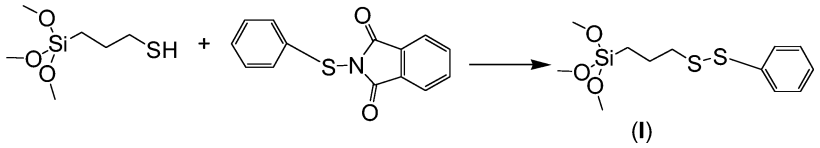

(**I**)

applied to a very small region, using a focused electron beam. EBL uses very tight beams (0.5−5 nm) of high-energy primary electrons to damage polymer resists such as poly(methyl methacrylate) (PMMA). Electron-beam damage is done not by the primary electrons, which, at 30−100 keV, have great penetrating power, but by the ∼10 eV secondary electrons, which are produced in abundance when a primary electron is captured by an atom in the substrate. The cleavage mechanism in PMMA involves radical and anionic mobile species that are generated by secondary electrons. Thus, electrons that are absorbed in one location can effectively diffuse through the polymer and cause cleavage at another site.[14] The cross section for absorption of a secondary electron is 80 times greater for sulfur than for carbon; therefore, the disulfide bond should be a locus for interaction with secondary electrons.[15] The disulfide, with its low reduction potential and weak bond, should also serve as a good trapping site for mobile radicals or anions and, hence, act as a locus of reductive cleavage.[16]

Disulfides are sensitive to reductive cleavage; however, they can also be oxidatively cleaved in solution by chemical or electrochemical oxidants. One way to deliver oxidizing power with high spatial resolution is AFM anodization.[17] In AFM anodization, a negative bias is applied to a conductive AFM tip under ambient conditions. Anodic oxidation of the embedded disulfide bonds would produce sulfoxides, sulfones, or sulfonic acids; DTT could later be used to cleave the unoxidized disulfide bonds in the remaining region to form a thiol-terminated complementary pattern. In either case, patterns of free thiol could be selectively derivatized with chemical cross-linkers and, hence, with dyes, biomolecules, nanoparticles, and so on.[18]

Embedded disulfide bonds have been formed on silicon substrates by Yee et al.; however, the smoothness and uniformity of the resulting SAMs were not sufficient for ultrahigh-resolution patterning.[19] A thiol-terminated monolayer was formed from a mercaptopropyltrimethoxysilane (MPTS) precursor, and the terminal thiol was allowed to exchange with a disulfide in solution to form disulfide bonds on the surface. However, the precursor was prone to multilayer formation, and the terminal thiol groups reacted with their neighbors to form undesired disulfide bonds, which have low reactivity and are unsuitable for further derivatization.[20]

Recently, we found that the sequential deposition of zirconium(IV) and organophosphonates with internal disulfide bonds allows the assembly of SAMs with embedded disulfide bonds.[21] There are no free thiol groups on the surface, and multilayer formation is not a problem. However, the sequential deposition is quite slow and introduces so many defects that the resulting monolayers are too rough for high-resolution patterning. Nonetheless, preliminary work demonstrated the susceptibility of the embedded disulfides to electron-induced damage. This paper describes a more tractable system that is based on SAMs of a siloxane derivative, phenyl(3-trimethoxysilylpropyl) disulfide (**I**), which forms smooth, continuous SAMs with embedded disulfides. These SAMs can be patterned by EBL or AFM anodization to form sub-50-nm features.

Results

Synthesis of Phenyl (3-Trimethoxysilylpropyl)-disulfide (I). The organosilane phenyl (3-trimethoxysilylpropyl)disulfide (**I**) was synthesized by refluxing *N*-(phenylthio)phthalimide with (3-mercaptopropyl)trimethoxysilane (MPTS) (as shown in Scheme 1). Compound **I**, which is a colorless oil, was purified by vacuum distillation. It is stable for months when kept in a drybox.

We also attempted to make the benzyl analogue of **I**; by adding a methylene unit, we hoped to alter the orientation of the terminal benzene ring.[22,23] Unfortunately, this compound could not be prepared in sufficient purity. Therefore, in this paper, we focus on compound **I** and the monolayer formed from it.

Preparation of Monolayer I. Preparation of a smooth monolayer is a key factor in the ultrahigh-resolution lithography of SAMs. Silicon wafers can provide a very smooth, flat substrate for siloxane growth (a root-mean-square (RMS) roughness of <1 Å over an area of 1 μm^2), but the wafer must be very clean and the growth solution must be very dry to obtain a siloxane SAM of comparable smoothness.[24] Wafers were cleaned with piranha solution to form a high density of Si−OH functional groups on the surface (∼20 $Å^2$ per Si−OH group),[25] as well as to remove organic and inorganic contaminants. Typically, a clean silicon wafer was refluxed in a dilute solution of compound **I** in dry octane for 30 min to form monolayer **I**.

Tapping-mode AFM of monolayer **I** formed on a 10-Å-thick silicon oxide surface shows that the monolayer is very smooth and uniform. The RMS roughness over a 5 $\mu m \times 5\ \mu m$ area of the film is 1.8 Å, which is similar to the roughness of a clean native oxide film. The ellipsometric thickness of monolayer **I** was 8.7 ± 0.5 Å, and the advancing water contact angle was 76°.

Modeling of Monolayer I. A schematic model of monolayer **I** on a silicon oxide substrate was built (see Scheme 2). First, the energy of molecule **I** was minimized in Chem 3D. Space-filling models of the energy-minimized molecule **I** are shown in Scheme 3. These molecules were packed on the surface, assuming a 0° tilt angle, as is

(14) Thompson, L. F.; Willson, C. G.; Bowden, M. J. In *Introduction to Microlithography: Theory, Materials, and Processing*; American Chemical Society: Washington, DC, 1983; p 124.
(15) Leiros, H.-K. S.; McSweeney, S. M.; Smalas, A. O. *Acta Crystallogr., Sect. D: Biol. Crystallogr.* **2001**, *57*, 488−497.
(16) Weik, M.; Ravelli, R. B. G.; Kryger, G.; McSweeney, S.; Raves, M. L.; Harel, M.; Gros, P.; Silman, I.; Kroon, J.; Sussman, J. L. *Proc. Natl. Acad. Sci. U.S.A.* **2000**, *92*, 623−628.
(17) Nyffenegger, R. M.; Penner, R. M. *Chem. Rev.* **1997**, *97*, 1195−1230.
(18) Mrksich, M. *Cell. Mol. Life Sci.* **1998**, *54*, 653.
(19) Yee, J. K.; Parry, D. B.; Caldwell, K. D.; Harris, J. M. *Langmuir* **1991**, *7*, 307−313.
(20) Ledung, G.; Bergkvist, M.; Quist, A. P.; Gelius, U.; Carlsson, J.; Oscarsson, S. *Langmuir* **2001**, *17*, 6056−6058.
(21) Wang, X.; Lieberman, M. *Langmuir* **2003**, *19*, 7346−7353.
(22) Lee, S.; Puck, A.; Graupe, M.; Colorado, R.; Shon, Y.-S., Jr.; Perry, S. S. *Langmuir* **2001**, *17*, 7364−7370.
(23) Wong, S.-S.; Takano, H.; Porter, M. D. *Anal. Chem.* **1998**, *70*, 5209−5212.
(24) Wang, Y.; Lieberman, M. *Langmuir* **2003**, *19*, 1159−1167.
(25) Wasserman, S. R.; Tao, Y.-T.; Whitesides, G. M. *Langmuir* **1989**, *5*, 1074−1087.

Scheme 2. Schematic Diagram of Monolayer I on Silicon Oxide Substrate

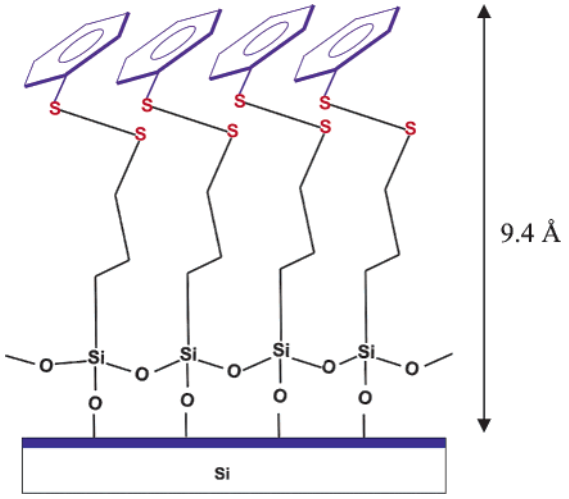

observed for most organosilanes.[26] The theoretical film thickness is 9.4 Å, which is similar to our ellipsometry measurement.

X-ray Photoelectron Spectroscopy Study of Monolayer I. X-ray photoelectron spectroscopy (XPS) was used to determine whether the monolayer was oxidized during deposition. A 500-nm-thick thermal oxide was grown on the substrate to eliminate a bulk plasmon band from elemental silicon.[21,27] This plasmon band overlaps with the S 2p peak at 168 eV and can be mistaken for oxidized sulfur. The S 2p region of the XPS spectrum of monolayer **I** (Figure 1a) shows an asymmetric peak, which was fitted as a coupled doublet at binding energies of 163.2 and 164.4 eV, respectively corresponding to the S $2p_{3/2}$ and S $2p_{1/2}$ signals of sulfur in the divalent oxidation state.[28] We conclude that monolayer **I** is not oxidized during deposition.

Coverage of Monolayer I. The coverage of monolayer **I** was estimated by comparing the ratio of nitrogen atoms to silicon atoms (N/Si) in a SAM of (3-aminopropyl)-triethoxysilane (APS) and the ratio of sulfur atoms to silicon atoms (S/Si) in a SAM of molecule **I**. This comparison assumes that electrons originating from the silicon substrate penetrate equivalent overlayers and are attenuated to a similar degree.

The thickness of the APS monolayer, as measured by ellipsometry, was 7 Å, and the ratio of N/(Si(0) + Si(IV)) was 0.066 ± 0.003. Monolayer **I** was 8.7 Å thick, and the ratio of S/(Si(0) + Si(IV)) was 0.067 ± 0.003. Considering that there is one N atom in APS and two S atoms in molecule **I**, the coverage of monolayer **I** is approximately half that of the APS monolayer, which is known to have a coverage of 25 $Å^2$ per molecule.[29] Thus, the coverage of monolayer **I** is ~50 $Å^2$ per molecule.

Angle-Resolved X-ray Photoelectron Spectroscopy Study of the Monolayer. To obtain more information about the monolayer structure and packing, angle-resolved XPS was used to study monolayer **I**. This technique is particularly useful in distinguishing continuous films from patchy films. As shown in Figure 2, at a takeoff angle of 90°, the Si 2p and Si 2s peaks from the

Scheme 3. Space-Filling Model of Compound I: (a) Side View and (b) Top View

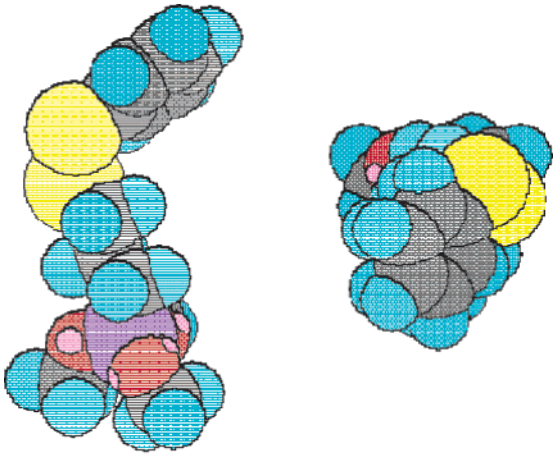

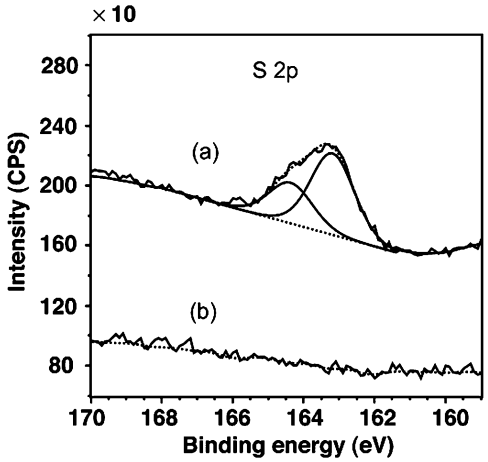

Figure 1. High-resolution X-ray photoelectron spectroscopy (XPS) spectra in the S 2p region: (a) monolayer **I** on a 500-nm-thick SiO_2/Si substrate, and (b) blank 500-nm-thick SiO_2/Si substrate.

silicon substrate are very strong, whereas, at a take-off angle of 15°, these two peaks have been enormously attenuated. In contrast, the C 1s peak has almost no change in intensity at these two different take-off angles. The attenuation of the substrate peaks suggests that monolayer **I** is a continuous film instead of a patchy film. If monolayer **I** were a patchy film, the Si 2p and Si 2s peaks would be much stronger at low take-off angles, because the Si 2p and Si 2s signals from the uncovered portion of the surface would not be attenuated at low take-off angles.

Angle-resolved XPS can also be used to estimate the thickness of the overlayer.[30] For a substrate with a uniform overlayer of thickness d, the ratio of XPS peaks from an atom in the overlayer to an atom in the substrate can be expressed as a function of the take-off angle (θ), as shown in eq 1:

$$\ln\left(\frac{R(\theta)}{K+1}\right) = \frac{d}{\lambda_k \sin\theta} \qquad (1)$$

where R is the ratio of the peak intensities of the overlayer to the substrate, K a constant, and λ_k the inelastic mean free path for a photoelectron in the substrate.

(26) Ulman, A. *Chem. Rev.* **1996**, *96*, 1533−1554.
(27) Zhang, Y. F.; Liao, L. S.; Chan, W. H.; Lee, S. T. *Phys. Rev. B* **2000**, *61*, 8298.
(28) Castner, D. G.; Hinds, K.; Grainger, D. W. *Langmuir* **1996**, *12*, 5083.
(29) Moon, J. H.; Kim, J. H.; Kim, K.-J.; Kang, T.-H.; Kim, B.; Kim, C.-H.; Hahn, J. H.; Park, J. W. *Langmuir* **1997**, *13*, 4305−4310.
(30) Huang, X.; Huang, H.; Wu, N.; Hu, R.; Zhu, T.; Liu, Z. *Surf. Sci.* **2000**, *459*, 183−190.

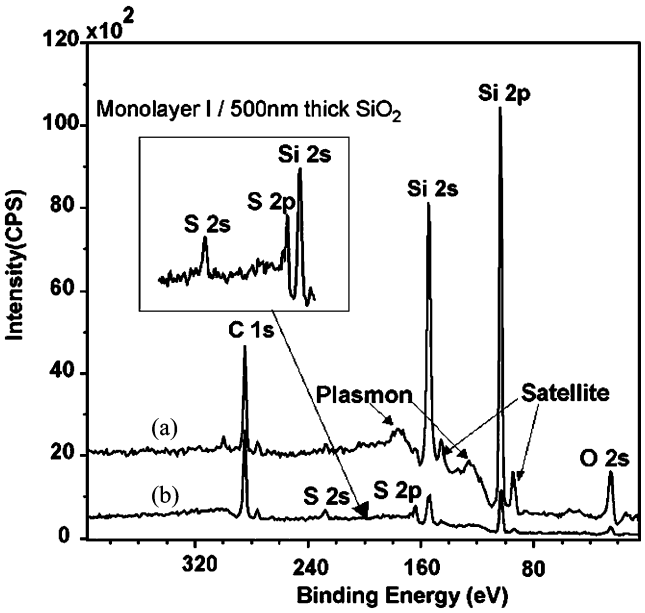

Figure 2. XPS survey scan of monolayer **I** formed on 500-nm-thick SiO_2 at take-off angles of (a) 90° and (b) 15°.

Table 1. Integrated Areas of S 2p Peaks and Si 2p Peaks from Monolayer I (500 nm Thick) at Different Take-Off Angles

take-off angle, θ (deg)	integrated area		$R(\theta)$
	$I_{S\ 2p}$	$I_{Si\ 2p}$	
90	411.6	22140.7	0.0186
75	538.6	22148.7	0.0243
60	815.7	21388.2	0.0381
30	1105.1	11315.5	0.0977
15	937.3	2648.5	0.354

The value of λ_k can be deduced from an empirical formula derived by Seah and Dench:[31]

$$\lambda_k = \frac{A_n}{E_k^2} + \frac{B_n}{E_k^{1/2}} \qquad (2)$$

where $A_n = 3.1$ and $B_n = 0.87$ for organic materials, and E_k is the kinetic energy of photoelectrons. For a Mg Kα source,

$$E_k = 1253.6 - E_B \qquad (3)$$

where E_B is the binding energy.

Using the data in Table 1, and assuming $K = 0.6$,[30] the plot of $\ln[R(\theta)/(K+1)]$ versus $1/(\sin\theta)$ is shown in Figure 3. These data fit a straight line, which is another indication that monolayer **I** is continuous and uniform. The slope d/λ_k is 0.149 ± 0.007.

From eqs 2 and 3, the value of λ_{Si} can be calculated to be 29.51 Å. Thus, the overlayer thickness d is 4.40 ± 0.21 Å. Considering the fact that the Si atoms from the siloxane cannot be differentiated from the substrate, the calculated overlayer thickness represents the distance from the S atoms to the Si atoms in the siloxane, which a Chem3D model estimates to be 4.2 Å.

Chemical Cleavage and Covalent Derivatization of Monolayer I. Disulfides react readily with DTT in basic solution. This chemical reactivity is preserved in the monolayer environment. Before DTT treatment, the S $2p_{3/2}$ peak of a monolayer of **I** was observed at 163.7 eV and the ratio of S to Si atoms on the surface was 0.034.

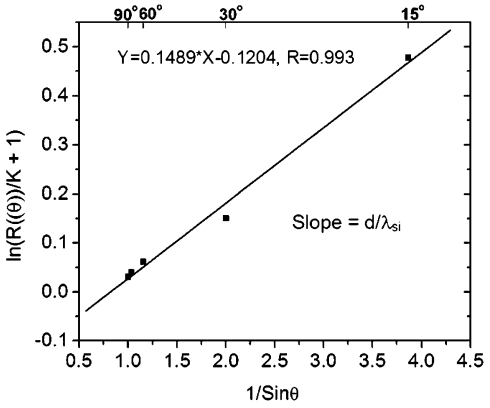

Figure 3. Plot of $\ln(R(\theta)/(K+1))$ vs $1/(\sin\theta)$ for monolayer **I** formed on 500-nm-thick silicon oxide.

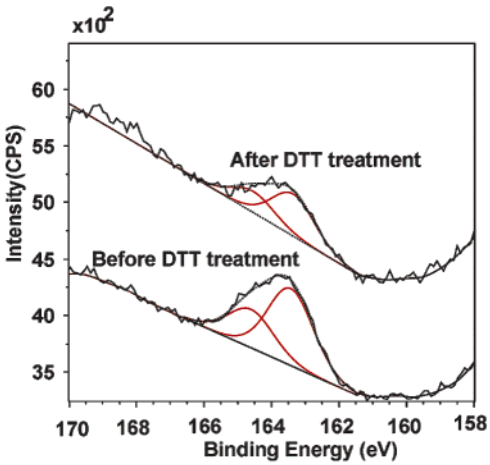

Figure 4. High-resolution XPS spectra on (a) monolayer **I** treated with DTT and (b) monolayer **I** without DTT treatment. In both cases, the substrate is 500-nm-thick silicon oxide, and the take-off angle is 30°.

After DTT treatment, the S $2p_{3/2}$ binding energy was virtually unchanged, but the S/Si ratio decreased to 0.015. (See Figure 4.) This 50% decrease in sulfur intensity suggests that DTT cleaves the embedded disulfide bonds with loss of the thiophenoxide fragment to solution.

Binding tests on monolayer **I** were conducted using 5,5′-dithiobis(2-nitrobenzoic acid) (DTNB), *N*-(1-pyrene)-maleimide, and the maleimide dye BODIPY 577/618. All these molecules are known to bind to thiols, but not disulfides, in solution. After cleavage of the disulfide with DTT, the monolayer, now presumably covered with SH groups, was exposed to solutions of DTNB, *N*-(1-pyrene)-maleimide, or BODIPY. DTNB, which is also known as Ellman's reagent, is widely used for colorimetric determination of the SH group in proteins.[32] However, it did not bind to the putative thiol-terminated SAM. Neither N 1s nor carbonyl C 1s (288 eV) peaks were present after treatment with DTNB.

After the freshly cleaved monolayer **I** was exposed to *N*-(1-pyrene)maleimide, a N 1s signal is observed at 400.5 eV and the C 1s signal develops a shoulder at ~288 eV, which is a binding energy that is consistent with the presence of a carbonyl group (Figure 5). The ratio between the areas of these two new peaks is 1.84, which is similar to the stoichiometric value of 2 in pyrene maleimide. The ratio of N 1s/S 2p is 1.52, which is higher than the expected value of 1, and the estimated surface coverage of *N*-(1-pyrene)maleimide is ~33 Å^2 per molecule; thus, some

(31) Seah, M. P.; Dench, W. A. *Surf. Interface Anal.* **1979**, *1*, 2.

(32) Jenke, D. R.; Brown, D. S. *Anal. Chem.* **1987**, *59*, 1509.

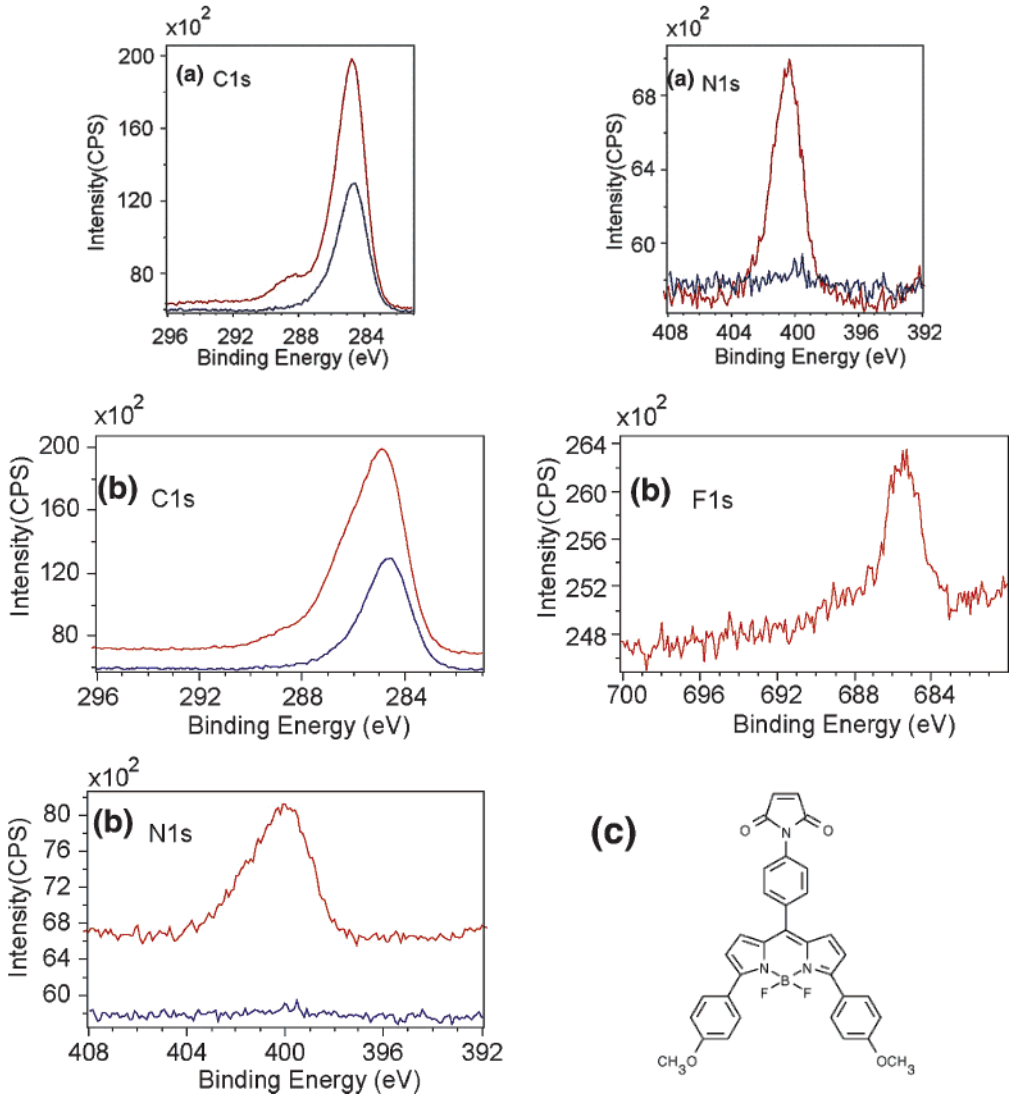

Figure 5. (a) High-resolution C 1s and N 1s XPS spectra of monolayer **I** before (blue curve) and after (red curve) DTT cleavage and binding of *N*-(1-pyrene)maleimide. (b) High-resolution C 1s and N 1s spectra of monolayer **I** before (blue curve) and C 1s, F 1s, and N 1s spectra after (red curve) DTT cleavage and binding of BODIPY 577/618. (c) Structure of BODIPY 577/618.

nonspecific binding or noncovalent interactions may occur. However, no detectable reaction was observed between the *N*-(1-pyrene)maleimide and control samples of monolayer **I** that had not been treated with DTT to cleave the disulfide.

BODIPY 577/618 also reacted with freshly cleaved monolayer **I**. As shown in Figure 5b, a broad N 1s signal appears at ~400 eV and can be fitted by two peaks at binding energies of 399.9 and 401.5 eV. The ratio of the two N peak intensities is 1.86. There are two different types of N atoms in BODIPY 577/618: the peak at the higher binding energy corresponds to the maleimide N atom, which is bound to two electron-deficient carbonyl groups, whereas that at the lower binding energy corresponds to the two pyrrole N atoms, which are bound to the anionic B atom. The C 1s signal can be fitted with three different components, at 284.6, 286.6, and 288.7 eV. The C signal at the highest binding energy is assigned to carbonyl C atoms. The ratio between carbonyl C atoms and N 1s is 0.98, which is slightly larger than the ideal ratio of 0.67. The ratio of F 1s to N 1s is only 0.37, which is smaller than the expected value of 0.67; this discrepancy could be due to XPS damage and the loss of fluorine. The ratio of N 1s to S 2p is 1.99, which indicates that approximately two out of three exposed S atoms bind a BODIPY molecule. The estimated surface coverage of BODIPY 577/618 is ~75 Å^2 per molecule. As a control, a monolayer of **I** that had not been treated with DTT was treated with BODIPY 577/618 solution. The XPS of this sample showed no F 1s, N 1s, or carbonyl C 1s signals.

Atomic Force Microscopy Anodization of Monolayer I. Disulfides can be oxidized to sulfonic acids by many chemical oxidants. Oxidizing equivalents can be delivered to a very small area of a surface by AFM anodization, in which a conductive AFM tip at a negative bias provides the oxidizing power. The water meniscus found at the tip/sample interface is crucial to this process, and it has been hypothesized that water oxidation products (e.g., hydroxyl radical) are the active oxidants.[33] AFM anodization was applied to monolayers of **I**, using an intermittant contact mode. At bias voltages of −10 and −11 V, the phase image (Figure 6b) shows hydrophilic lines with line widths of 20 and 30 nm, respectively. However, on the topographic image (Figure 6a), only the line corresponding to −11 V is visible as a raised feature of 1.0 Å. These changes in surface polarity and topography

(33) Avouris, Ph.; Hertel, T.; Martel, R. *Appl. Phys. Lett.* **1997**, *71*, 285−287.

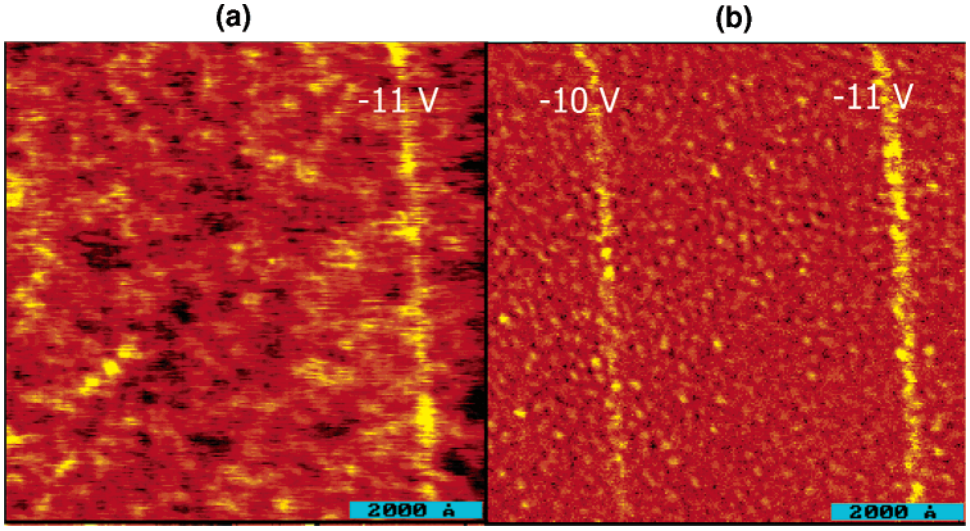

Figure 6. Tapping-mode AFM image of two vertical lines drawn sequentially with a conductive silicon tip on the phenyl(3-trimethoxylsilylpropyl)disulfide monolayer (**I**): (a) topography image and (b) phase image. The voltage applied on the tip has been labeled on the image, and the writing speed is 6.8 μm/s.

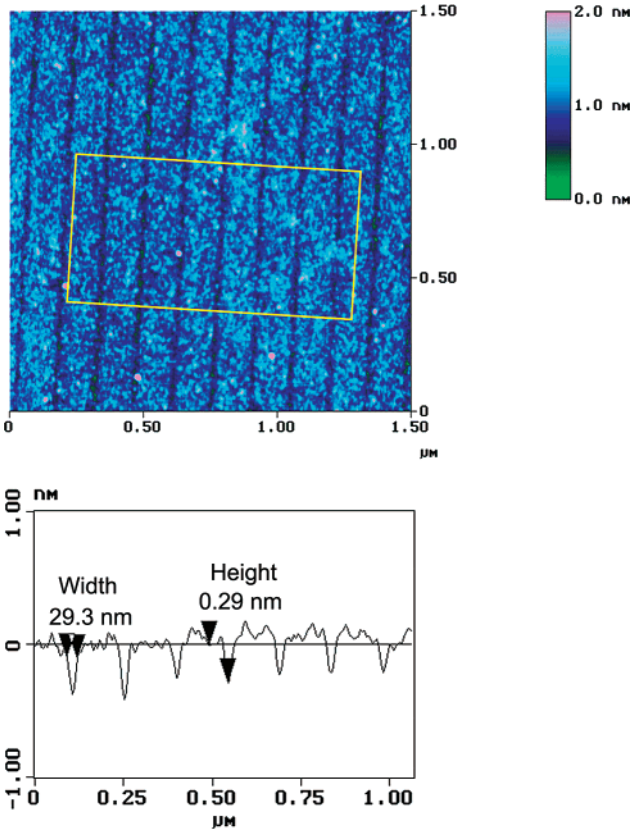

Figure 7. Tapping-mode AFM image of the line pattern generated by a 30-kV focused electron beam with a line dose of 1.1×10^{-8} C/cm. The profile is the average cross section in the box.

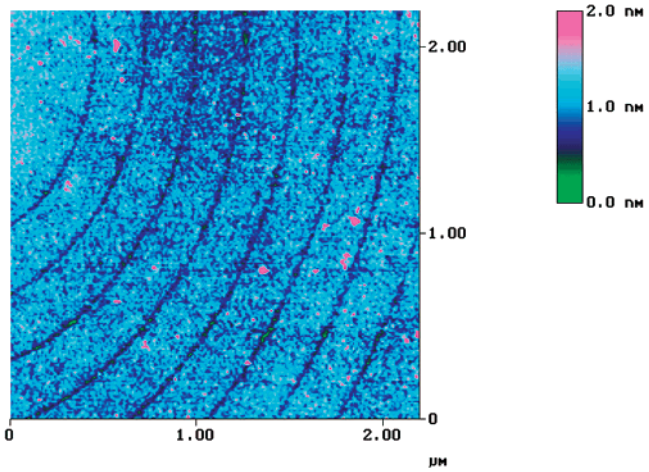

Figure 8. Tapping-mode AFM image of the circle pattern generated by 30-kV focused electron beam with a line dose of 1.4×10^{-8} C/cm.

could be repeated over larger areas of the wafer by scanning with the AFM tip held at the anodizing voltage.

Electron Beam Lithography of Monolayer I. EBL is a well-established technique that is capable of high-resolution patterning of organic resists. Figure 7 shows a tapping-mode AFM image of a grating on a 150-nm pitch. It was generated by electron-beam direct writing on the monolayer of **I** with an accelerating voltage of 30 kV. Each line was written in a single pass of the electron beam at a line dose of 1.1×10^{-8} C/cm. Measurement of the cross-sectional profile indicates that these lines have a line width of 35.2 ± 4.1 nm and consist of trenches with a depth of 2.8 ± 0.4 Å, measured from the baseline of the surrounding SAM surface.

To test the reproducibility of the EBL process, another sample was prepared and patterned by EBL, using a line dose of 1.4×10^{-8} C/cm. As shown in Figure 8, a series of circles was generated by electron-beam direct writing with an accelerating voltage of 30 kV. Each line was written in a single pass of the electron beam at a line dose of 1.4×10^{-8} C/cm. The average depth is ~3 Å, and the line width is ~30 nm.

To gain more information about the chemical change in the trenches, the electron beam was defocused to a diameter of 100 nm, and the same dose as that previously applied (1.4×10^{-8} C/cm) was used to form circular patterns. From the tapping-mode AFM image (Figure 9a), 100-nm-wide trenches were formed. The trench depth was ~3 Å, which is the same as that of the 30-nm-wide trenches. A series of carbonaceous build-up spots were also generated by holding the beam at the same position for 1 s (1.68×10^{-11} C per spot). These "contamination" spots consist of condensed carbonaceous materials from the decomposition of oil from the vacuum pumps, and they are known to be hydrophobic in nature.[34] The diameter of the

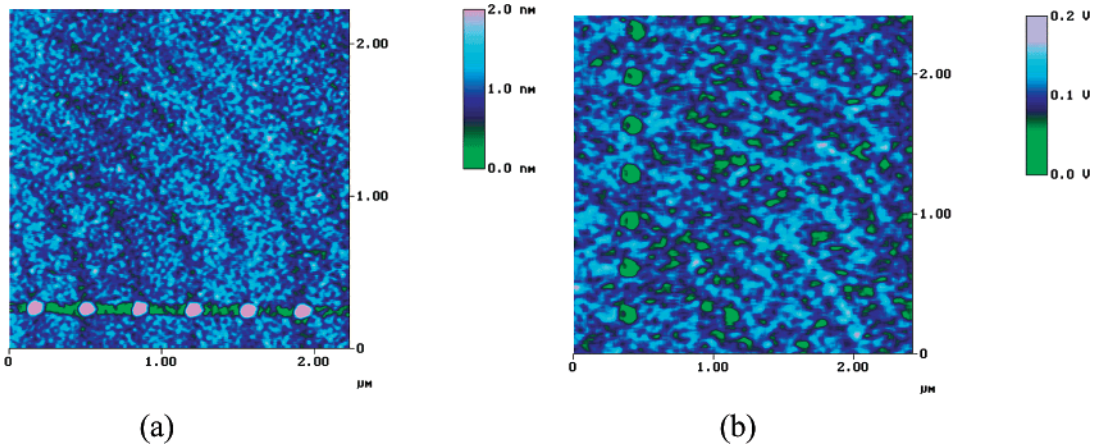

Figure 9. AFM images of the circular pattern generated by a 30-kV electron beam with a line dose of 1.4×10^{-8} C/cm: (a) tapping mode and (b) friction mode (image rotated by −90°). Spots are carbonaceous buildup, with a dose of 1.68×10^{-11} C/spot.

contamination spots was 100 nm, and their height was 2 nm.

Next, this sample was imaged with lateral force microscopy (LFM). LFM measures the lateral deflection (twisting) of the cantilever while the tip scans the sample surface. The cantilever will twist more strongly as the tip navigates on the higher-friction areas. Hydrophobic SAM surfaces have lower friction, whereas hydrophilic SAM surfaces have higher friction.[35] Using the contamination spots as a marker, it is possible to locate the trenches. As shown in Figure 9b, the hydrophobic contamination spots have lower friction than the background SAM of molecule **I**, whereas the trenches have higher friction.

X-ray Photoelectron Spectroscopy Damage Study. To clarify the mechanism of EBL damage on the monolayer, it would be interesting to perform an XPS study of the area exposed to the electron beam. However, it is impossible to characterize fine-feature exposure by XPS, because an irradiation area of up to several square centimeters is required for the analysis. In the EBL study, fine-feature exposures were performed on a Hitachi S-4500 cold-cathode field-emission scanning electron microscopy (SEM) system. This SEM equipment is not suitable for wide-area irradiation, because of its low throughput.[36] An alternative method for wide-area exposure is to use the X-ray beam to damage the monolayer. This type of damage has been studied by other workers, because it is a potential problem whenever thin films are studied by XPS.

XPS damage studies were conducted on a monolayer of **I** using the X-ray source of our XSAM800 system to irradiate the samples. A take-off angle of 45° was used for this study. Sample damage was monitored by collecting XPS data at specified intervals. Figure 10 shows the change of S 2p intensity, relative to X-ray exposure time; the inset in Figure 10 shows the natural logarithm of the intensity versus time. The S 2p signal intensity is reduced exponentially until it has lost 57% of its initial strength after 3 h of damage. Thereafter, the rate of loss of S 2p intensity slows. Figure 11 shows high-resolution S 2p spectra of monolayer **I** after 0, 1, and 3 h of XPS damage.

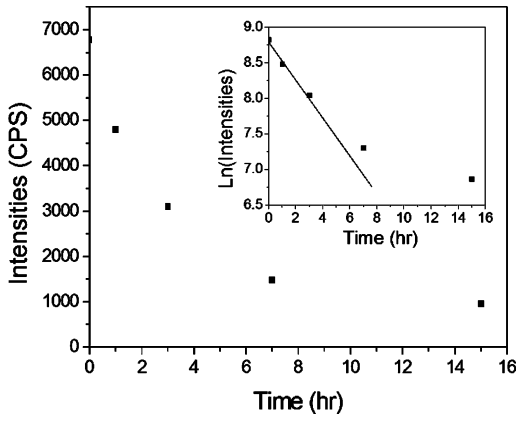

Figure 10. Change of S 2p intensity with X-ray exposure time. Intensities are the integrated peak areas, corrected for the relative sensitivity factor (RSF).

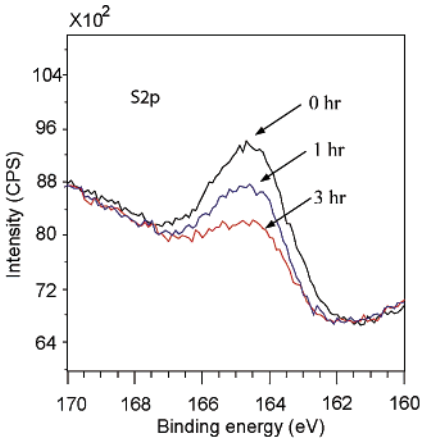

Figure 11. XPS S 2p spectra of monolayer **I**. Black curves represent the fresh monolayer **I**, blue curves represent monolayer **I** after 1 h of in situ XPS damage, and red curves represent monolayer **I** after 3 h of in situ XPS damage.

Clearly, there is no peak in the oxidized S 2p region (~168 eV). The intensity of the C signal was reduced by 11% after 1 h of exposure, did not change after 2 h of further exposure (a total of 3 h), and then started to increase; the C 1s intensity after 15 h of exposure was 10% higher than that with 0 h of exposure.

Pattern Transfer. To demonstrate that the patterns formed by EBL of monolayer **I** can be used as a template for selective chemical binding, patterns were treated with 10 mM *N*-(1-pyrene)maleimide, to derivatize any free

(34) McCord, M. A.; Rooks, M. J. In *Handbook of Microlithography, Microfabrication and Microsystems*; Rai-Choudhury, P., Ed.; SPEI Press: Washington, DC, 1997.

(35) (a) Wilbur, J. L.; Biebuyck, H. A.; MacDonald, J. C.; Whitesides, G. M. *Langmuir* **1995**, *11*, 825−831. (b) Maoz, R.; Cohen, S. R.; Sagiv, J. *Adv. Mater.* **1999**, *11*, 55−61.

(36) Typically, the exposure dose for PMMA is 100 μC/cm^2 and the beam current for the Hitachi S-4500 system is 10 pA. Exposure of an area of 1 cm^2 would require 100 μC/10 pA = 10^7 s = 3000 h.

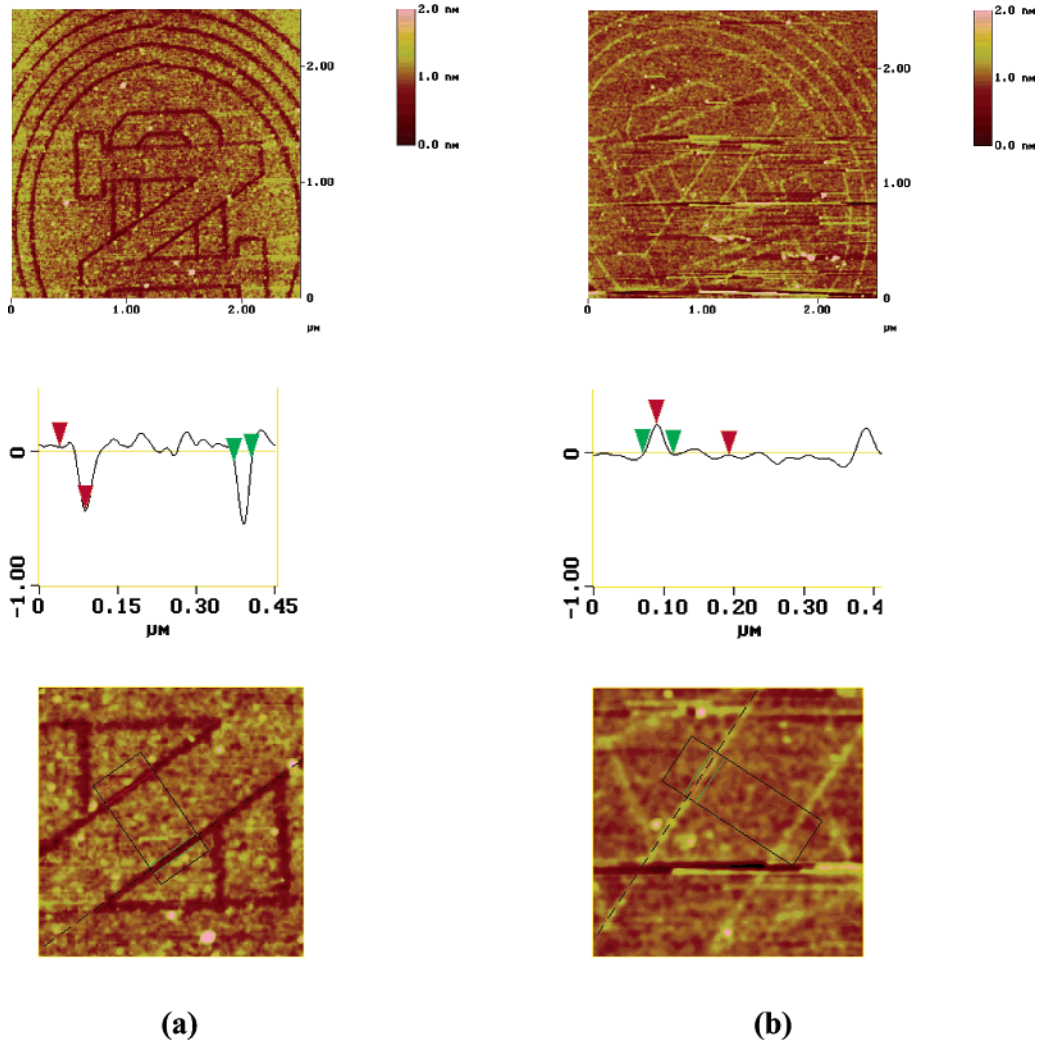

Figure 12. Tapping-mode AFM image of the sub-50-nm pattern generated by a 30-kV focused electron beam with a line dose of 7.0×10^{-9} C/cm (a) before and (b) after treatment with *N*-(1-pyrene)maleimide; the boxes that were integrated for the cross sections are shown in the enlarged images at the bottom.

thiols formed during EBL exposure. Before treatment (Figure 12a), the trench depth was 4.8 Å and the line width was ~35 nm. After *N*-(1-pyrene)maleimide treatment (Figure 12b), the trenches were "filled in", with an apparent height of 2.3 Å and a width of 44 nm. The average height change of the trench region is ~7 Å; the rest of the SAM surface seems to be unaltered. This result suggests that *N*-(1-pyrene)maleimide molecules attach selectively in the patterned region.

Discussion

Monolayer Structure. The embedded disulfide bond affects both the packing and coverage of the SAM of **I**. The surface area occupied by molecule **I** (as estimated by XPS) is ~50 Å^2 per molecule. This is approximately twice the area per molecule required for SAMs of aminopropyltrimethoxysilane (APS). The disulfide is sterically small, but it has a preferred dihedral angle of 91°,[37] which induces a bend in the hydrocarbon portion of molecule **I**. This kink has a dramatic impact on the orientation of the benzene rings. The theoretical thickness of the monolayer if the disulfide is straightened out (to a dihedral angle of 180°) is ~13 Å, whereas if the disulfide kink is included, it is 9.4 Å, which is similar to our ellipsometric measurement of 8.7 ± 0.5 Å. Instead of standing upright, the benzene rings must lie almost flat, similar to shingles on a roof. In this conformation, the projected area of molecule **I** is also approximately twice that of the projected area of APS. Thus, the relatively low coverage of molecule **I** is quite reasonable. The advancing water contact angle for monolayer **I** is 76°, similar to the 86° contact angle of highly oriented pyrolytic graphite (HOPG).[38] The decreased contact angle, relative to HOPG, indicates that SAMs of **I** may be disordered. However, XPS indicates that the films are continuous, not patchy, and AFM images show that the monolayer surface is smooth and uniform, with an RMS roughness of 1.8 Å over an area of 1 μm^2.

Chemical Reactivity. When monolayer **I** is soaked in a basic solution of DTT, 50% of the S 2p signal disappears from the XPS. Based on the known ability of DTT to cleave disulfides to thiols, the disulfide bond that is embedded in the monolayer of **I** must have been cleaved, leaving behind a thiol-terminated SAM. However, dithionitrobenzoic acid (DTNB, Ellman's reagent) does not attach to the freshly cleaved surface. The simplest explanation is that the thiol groups on the surface of the SAM are too sterically congested to access the backside of the DTNB disulfide, although the surface thiols could form disulfides with each

(37) Jiao, D.; Barfield, M.; Combariza, J. E.; Hruby, V. J. *J. Am. Chem. Soc.* **1992**, *114*, 3639.

(38) Adamson, A. W., Gast, A. P. *Physical Chemistry of Surfaces*; Wiley−Interscience: New York, 1997.

other. The former situation is the most likely explanation, because two maleimide dyes, *N*-(1-pyrene)maleimide and BODIPY, are able to react with monolayer **I** after the internal disulfide has been cleaved by DTT. Maleimides do not react with disulfides, but they do readily undergo Michael reactions with thiols. The Michael acceptor site is well-exposed in both maleimide dyes; therefore, this reaction should be feasible for a thiol, even in a sterically congested environment such as a SAM.

AFM Anodization. AFM anodization of the monolayer of **I** involves two competing processes: a degradation of the organic resist and an anodization reaction of the silicon substrate. In experiments that were performed on SAMs of octadecyltrichlorosilane (OTS) on silicon, anodization of the silicon substrate causes growth of a "wall" of silicon oxide.[39] In monolayers of **I**, cleavage of the disulfide bonds in the monolayer could offset the height increases caused by SiO_2 formation. However, the presence of two types of chemical changes is not optimal for specific chemical derivatization of the patterned areas. Several factors such as humidity, voltage applied to the tip, speed of writing, and tip−sample distance are known to affect the AFM anodization process;[40] thus, it may be possible, by optimizing the anodization conditions, to favor one process over the other.

Effect of Electron Beam Lithography on the Embedded Disulfide Bonds. To understand the effect of EBL on the monolayer of **I**, a series of experiments was performed. Each of them reveals one aspect of the chemical process. According to the tapping-mode AFM result, the observed depth of the trench formed by EBL is ∼3 Å. This result is consistent with the cleavage of disulfide bonds, considering that the model shown in Scheme 2 suggests the thickness change after cleavage of disulfide bonds should be 3.2 Å. From LFM, we observe that the trench region is hydrophilic, whereas the remaining phenyl-terminated SAM is slightly hydrophobic. This indicates the formation of polar functional groups, such as SH or SO_3H_2. On the basis of these results, EBL causes the cleavage of embedded disulfide bonds in the SAM. The thiophenol fragment is lost to vacuum; however, the siloxane fragment remains attached to the silicon surface.

XPS damage simulates wide-area electron-beam damage. Graham et al., in their studies of XPS damage on trifluoroacetamide-terminated monolayers, concluded that electrons, not X-rays, are the principal cause of damage to the monolayer.[41] The electrons are generated through the interaction of an X-ray photon with an inner-shell electron of an atom. Seshadri et al. also reported that X-ray damage on the octadecyltrichlorosilane monolayer induces the same fundamental types of changes as electron-beam damage.[42] XPS damage of monolayer **I** provides additional information on the chemical changes that occur during EBL. The main effect of X-ray exposure was the loss of sulfur. In particular, during the first 3 h of exposure, the integrated intensity of the S 2p peaks decreased exponentially, to ∼50%. Throughout the entire exposure period, no oxidized sulfur was detected. These results suggest that electrons cleave the embedded disulfide bonds reductively, to eventually form SH terminal groups. The intensity of the S 2p signal continued to be reduced upon further X-ray exposure; however, the rate of reduction was much slower, so the decrease in signal intensity could be due to further damage to the terminal thiol groups, leading to alkane and H_2S. In the initial 3 h, when the sulfur loss was at its highest rate, the C 1s signal lost only 10% of its intensity, which is low if it is to correspond to the loss of phenyl groups. However, this value is not so unreasonable, taking the expected carbonaceous buildup in the vacuum chamber into consideration. Extended exposure of any surface to an X-ray beam (or an electron beam) causes deposition of "adventitious carbon", which is an ill-defined carbonaceous material thought to originate from the cracking of pump oil. Indeed, extended exposure to the X-ray beam caused a steady buildup of the C1s signal at 284.6 eV.

Chemical tests confirm the nature of the damage caused by EBL of monolayers of **I**. After exposure to the electron beam, the putative thiol-terminated trench regions bind *N*-(1-pyrene)maleimide, whereas the unexposed regions do not react with the maleimide. Because maleimide compounds selectively react with RSH groups but not with RSSR or RSO_3H, the exposed area contains a high density of SH terminal groups.

Mechanism of Electron-Beam Damage. Previous studies of electron-beam damage on hydrocarbon monolayers have shown C−H bond scission. Seshadri et al. studied electron-beam-induced damage in self-assembled octadecyltrichlorosiloxane monolayers on oxide-covered silicon.[42] They noticed that the major effect of irradiation was the loss of H atoms via the cleavage of C−H bonds, which lead to orientational and conformational disorder of the chains, the desorption of materials, and the formation of C=C bonds in the fragments remaining on the surface.[42] Recently, Gölzhäuser et al. investigated electron-induced damage in well-ordered monolayers of an aromatic biphenylthiol.[43] They found that, when the monolayers were irradiated with 50-eV electrons, C−H cleavage occurred, which was then followed by cross-linking between neighboring phenyl units.[43] Because trenches have formed in our system, it is not likely that the neighboring phenyl units have cross-linked. In addition, monolayers of **I** contain disulfide bonds, which open up a new manifold of monolayer reactivity.

According to previous radiation biology studies, disulfide bonds are likely to trap radicals, which usually results in cleavage of the disulfide.[44] Recently, Weik et al. reported that synchrotron radiation damage of the enzyme *Torpedo californica* acetylcholinesterase is highly specific. The radiation selectively breaks disulfide bridges in the enzyme, with more solvent-exposed disulfides being broken at a faster rate.[16] This is considered to be evidence for trapping of reactive species in the solvent, rather than direct cleavage of the disulfide by the X-rays.

During EBL of monolayers of **I**, the tightly focused primary beam (30 keV) results in large numbers of secondary electrons (∼10 eV) when it interacts with the substrate. Absorption of these secondary electrons by the disulfide (which has a much larger cross section for capturing an electron than a typical C−H bond) initiates the damage. Secondary electrons, which react with C−H bonds in the SAM, will create reactive radicals, which the disulfides may also be able to trap, again initiating cleavage of the disulfide. The S−S bond breaks, leaving a thiolate or a thio radical attached to the surface and a

(39) Lee, W. B.; Oh, Y.; Kim, E. R.; Lee, H. *Synth. Met.* **2001**, *117*, 305.

(40) Sugimura, H.; Nakagiri, N. *J. Photopolym. Sci. Technol.* **1997**, *10*, 661.

(41) Graham, R. L.; Bain, C. D.; Biebuyck, H. A.; Laibinis, P. E.; Whitesides, G. M. *J. Phys. Chem.* **1993**, *97*, 9456−9464.

(42) Seshadri, K.; Froyd, K.; Parikh, A. N.; Allara, D. L.; Lercel, M. J.; Craighead, H. G. *J. Phys. Chem.* **1996**, *100*, 15900−15909.

(43) Gölzhäuser, A.; Geyer, W.; Stadler, V.; Eck, W.; Grunze, M.; Edinger, K.; Weimann, Th; Hinze, P. *J. Vac. Sci. Technol. B* **2000**, *18*, 3414.

(44) Sonntag, C. V. *The Chemical Basis of Radiation Biology*; Taylor and Francis: London, New York, 1987.

thiophenol radical or thiophenolate group, which will be lost to vacuum. The reactive fragments are quenched by H atoms (abstracted from neighboring molecules) or by protons; this quenching may occur when the sample is removed from the ultrahigh-vacuum (UHV) chamber.

Summary

A self-assembled monolayer (SAM) of phenyl (3-trimethoxysilylpropyl) disulfide (**I**) was used successfully as an engineered ultrathin resist for atomic force microscopy (AFM) anodization and electron-beam lithography (EBL) direct writing. AFM anodization formed lines as narrow as 20 nm on the monolayer. EBL with an accelerating voltage of 30 kV generated chemical patterns on this monolayer that had a resolution of 30 nm. According to AFM topographic and friction images, X-ray photoelectron spectroscopy (XPS) damage simulation, and chemical rebinding tests, these changes are consistent with cleavage of the disulfide bonds to form sulfhydryl groups.

Experimental Section

1. Materials. *N*-(Phenylthio)phthalimide, 5,5′-dithiobis(2-nitrobenzoic acid) (DTNB) , and *N*-(1-pyrene)maleimide were commercially available and was used without purification. All three compounds were obtained from Aldrich. 4,4-difluoro-3,5-bis(4-methoxyphenyl)-8-(4-maleimidylphenyl)-4-bora-3a,4a-diaza-s-indacene (BODIPY 577/618 maleimide, $C_{33}H_{24}BF_2N_3O$) was purchased from Molecular Probes, Inc., and a stock solution in dry dimethylsulfoxide (DMSO) was stored in a freezer in a drybox. (3-mercaptopropyl)trimethoxysilane (MPTS) was purchased from Aldrich and was purified by vacuum distillation prior to use. Benzene and toluene were dried over sodium. Other organic solvents were used directly as received.

2. Instrumentation. ^{1}H NMR spectra were taken on a Varian Unity+ 300 instrument. Mass spectra were obtained on a JEOL model JUS-AX505 HA mass spectrometer, using FAB+ ionization. IR spectra were taken as thin films (from evaporation of a dichloromethane solution) on KBr plates and were analyzed on a Perkin−Elmer model Paragon 1000 FT-IR spectrometer.

3. Syntheses. *3.1. Phenyl(3-trimethoxysilylpropyl)disulfide (**I**).* This compound was synthesized by refluxing 5.37 mL (30 mmol) of vacuum-distilled MPTS (Aldrich) and 8.70 g (34 mmol) *N*-(phenylthio)phthalimide (Aldrich) in 30 mL of dry benzene overnight. When the reaction mixture had cooled, a white precipitate was removed by filtration. Compound **I** (3.75 mL (70%)) was obtained by vacuum distillation at a temperature of 110 °C and a pressure of 10−15 Torr. The pure compound **I** was stored in a drybox. ^{1}H NMR($CDCl_3$): 0.73 (m, 2H), 1.80 (m, 2H), 2.75 (t, $J = 7.2$ Hz, 2H, S−CH_2), 3.54 (s, 9H, Si−OCH_3), 7.23 (t, 1H), 7.31 (t, 2H), 7.53 (d, 2H). MS(FAB+): calcd., 304.6023; found, 304.6020. IR (KBr pellet): 2941.1(s), 2922.4(s), 2838.0(s), 1579.6(w), 1474.8(w), 1438.3(w), 1187.4(s), 1082.7(vs), 1017.5(w), 811.1(s), 738.2(s), 685.6(w), 456.3(w). Previously, Stjernlof et al. reported the synthesis of compound **I**, using diethyl azodicarboxylate (DEAD) as the oxidizing reagent to form an intermediate with MPTS. The intermediate then reacts with thiophenol to form **I** in 40% yield.[45]

*3.2. N-(Benzylthio)phthalimide (**II**).* This intermediate was synthesized by following the method established by Eberlein and Powell.[46] *N*-Bromophthalimide (11.3 g, 50.0 mmol) and dibenzyl disulfide (12.3 g, 50.0 mmol) were refluxed for 0.6 h in 50 mL of dry toluene. The red reaction mixture was allowed to cool to room temperature before the addition of 150 mL of hexane. The crystals formed were filtered off and recrystallized from hot EtOH. Yield, 8.6 g (66%); mp, 168 °C.

*3.3. Benzyl(3-trimethoxysilylpropyl)disulfide (**III**).* *N*-(Benzylthio)phthalimide (8.6 g, 32 mmol) and 5.49 mL (30.7 mmol) of vacuum-distilled MPTS (Aldrich) were refluxed for 24 h in 50 mL of dry toluene. When the reaction mixture had cooled, a white precipitate was removed by filtration. Purification was attempted by vacuum distillation. Compound **III** (3.00 mL, 95% pure (based on NMR)) was obtained by vacuum distillation at a temperature of 90−110 °C and a pressure of 17 Torr. The impurity in the mixture was the disulfide dimer of MPTS, as indicated by its NMR and mass spectroscopy (MS); this impurity could not be removed by chromatography or distillation.

3.4. Monolayer Formation. Silicon wafers (Wafernet, Inc.; 0.5-mm-thick Si(100), with one side polished, *p*-type, B-doped, with a resistivity of 10−20 Ω cm) were cut into 1 cm × 1 cm pieces, cleaned with piranha solution (concentrated H_2SO_4 and 30% H_2O_2, 3:1 in volume) for 15 min, and then rinsed completely with water and blown dry with N_2. (CAUTION: Piranha solutions are strong oxidants and should be used with extreme care, and in the absence of organic solvents!) The wafer was then dipped into a 10:1 DI H_2O:HF solution for 30 s to remove the original native silicon oxide. RCA cleaning procedures were performed next; the silicon wafers were first cleaned[47] in a NH_4OH:H_2O_2:H_2O (1:1:5) solution at 70 °C for 15 min, rinsed with water for 5 min, then immersed in a HCl:H_2O_2:H_2O (1:1:5) solution at 70 °C for 15 min, rinsed again with water for 5 min, and finally dried with flowing N_2. Silicon wafers were cleaned and prepared just prior to use. SAMs of **I** were formed on the native oxide by immersing the small pieces of wafers in an octane solution of 5 mM **I** and refluxing for 30 min, followed by ultrasonicating for 10 min in toluene, rinsing with toluene for 1 min, then ultrasonicating for 10 min in CH_2Cl_2, rinsing again with CH_2Cl_2 for 1 min, and then blowing dry in a stream of N_2. Some samples were also prepared on 500-nm-thick silicon oxide, which was formed by thermal oxidization in an oxygen environment at 1200 °C for 3 h. In this case, the substrate was cleaned with piranha solution at 70 °C for 15 min and the monolayer growth process was the same.

3.5. Ellipsometric Thickness Measurement. Ellipsometric measurements were made with a Rudolph model AutoEL III ellipsometer equipped with a (He−Ne laser) analyzing light (wavelength of 6328 Å) operating at an incident angle of 70°. Measurement of each piece of the clean silicon wafer before monolayer growth yielded the thickness of the native oxide layer. Subsequently, the thicknesses of monolayers were determined using a two-layer model (adsorbate/SiO_2/Si) with the previously determined thickness for the native oxide layer and an assumed refractive index of 1.50 for the absorbate. On each sample, at least five different locations were measured and the results were averaged.

3.6. Contact Angle Measurement. Contact angles were measured on a Kruss model G10 goniometer. Advancing and receding angle measurements were made with the captive drop technique. Typically, a 5 μL droplet of 18 MΩ water was added onto the sample surface. The advancing contact angle was measured when the volume of the droplet was increased without increasing the solid/liquid interfacial area. Similarly, the receding angle was measured as the volume of the droplet was reduced without changing the solid/liquid interfacial area.

3.7. X-ray Photoelectron Spectra. XPS spectra were obtained using a Kratos model XSAM 800 spectrometer with nonmonochromatic Mg Kα radiation at 1253.6 eV (144 W, 40 eV pass energy). The pressure in the spectrometer was typically 10^{-8} Torr. Binding energies were referenced to Si 2p at 99.0 eV or SiO_2 at 103.3 eV. After subtraction of a linear background, all spectra were fitted using 70% Gaussian/30% Lorentzian peaks, taking the minimum number of peaks consistent with the best fit. The S 2p peak was fitted using linked doublet peaks (peak width not constrained, S $2p_{1/2}$/S $2p_{3/2}$ area ratio of 0.5, spin−orbit coupling of 1.2 eV). The take-off angle is defined as the angle between the analyzer axis and the sample surface plane. The take-off angle is 90°, unless specified otherwise. For angle-resolved XPS measurements, samples were mounted onto a sample holder and then the holder was placed on an *XYZ* manipulator that was present in the sample analysis chamber. The *XYZ* manipulator provided rotation of ±180° about the *x*-axis.

3.8. Chemical Cleavage and Rebinding. Monolayer **I** on Si(100) substrates was soaked in a pH 9.0 *tris*-HCl buffer that contained

(45) Stjernlof, P.; Jonsson, U.; Ronnberg, I. *Tetrahedron Lett.* **1990**, *31*, 5773.

(46) Eberlein, G. A.; Powell, M. F. *J. Am. Chem. Soc.* **1984**, *106*, 3309.

(47) Kern, W.; Puotinen, D. A. *RCA Rev.* **1970**, *31*, 187.

100 mM DTT for 1 h. The reaction was performed in the hood at room temperature. For comparison purposes, two fresh monolayer **I** samples were prepared in parallel. One sample was treated with 100 mM DTT in pH 9 *tris*-HCl buffer (1.0 M) for 1 h, and the other sample was kept in air as a control sample. The cleavage process was followed by XPS, and a 30° take-off angle was used to enhance the signal-to-noise ratio of the S 2p peak.

After treatment with 100 mM DTT in pH 9.0 *tris*-HCl buffer for 1 h, rebinding was attempted using 10 mM 5,5′-dithiobis-(2-nitrobenzoic acid) in pH 7.5 *tris*-HCl buffer for 1 h. Rebinding was also attempted using 10 mM *N*-(1-pyrene)maleimide or 1 mM BODIPY in CH_2Cl_2 for 1 h. To control the pH of the bulk solutions, 5 mL of pH 7.5 *tris*-HCl buffer was added to the aforementioned CH_2Cl_2 solution as a second layer. After treatment, the samples were rinsed completely with CH_2Cl_2 and water and then dried in a stream of N_2.

3.9. Atomic Force Microscopy. AFM was performed using a Nanoscope III (Digital Instruments). The images were taken in tapping mode with 125-μm narrow-leg sharpened silicon nitride tips (Nanoprobe SPM tips, type TESP, with a frequency of ~300 kHz). The fast scan direction was from left to right. Scan rates for the experiments were typically 1 Hz. The root-mean-square (RMS) roughness was calculated on a 25 μm^2 area using DI software. Some images were taken in lateral-force mode with 250-μm narrow-leg sharpened silicon tips (Nanoprobe).

AFM anodization was performed by applying a bias ranging from −8 V to −12 V to the tip of a Molecular Imaging PicoSPM AFM system that was equipped with a model SPM 1000 controller (RHK Technology). The relative humidity was 40%−50%. The pattern was drawn on the film with a conductive tapping-mode silicon tip (Veeco Metrology, Part No. ULNC-AUHW; resonant frequency of ~100 kHz) that was operating in tapping mode. After AFM anodization, the bias was removed and the image was acquired in tapping mode with the same AFM tip.

3.10. Electron-Beam Lithography. EBL was performed with a Hitachi model S-4500 cold-cathode field-emission scanning electron microscopy (SEM) system controlled by a custom pattern generator (V5.2 system). The exposure was conducted at an accelerating voltage of 30 kV and a beam current of 10 pA. To locate an exposure area precisely, a locator pattern was made on the silicon wafer before monolayer growth. An SEM image of the central portion of the locator is shown in Figure 13. The locator pattern is made by photolithography, followed by reactive-ion etching on the silicon wafer. The darker area is smooth native silicon oxide and the lighter region is rough etched silicon oxide.

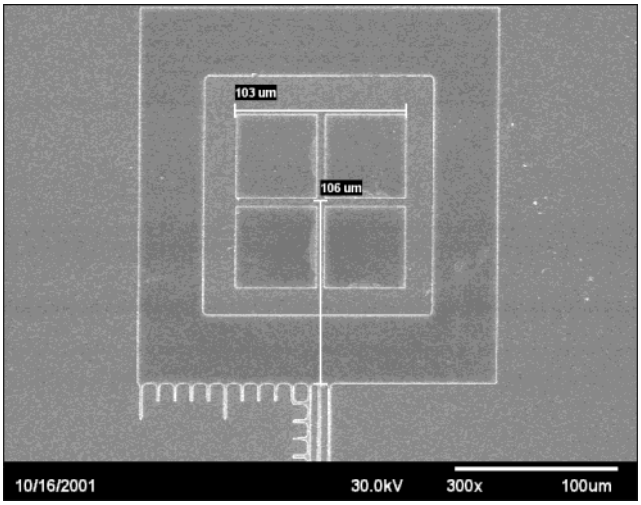

Figure 13. SEM image of the locator for electron beam lithography. The slightly darker four squares are smooth native silicon oxide, and the scale bar is 100 μm long.

The edges of the pattern appear brighter due to SEM edge effects. The height difference between the etched area and the smooth silicon oxide area is ~50 nm. Sharp edges on the marker pattern were used for precise focusing of the electron beam. The beam could be focused to a diameter of <2 nm, judging by the ability to resolve features of the line edges.

3.11. X-ray Photoelectron Spectroscopy Damage. XPS damage was performed using a Kratos model XSAM 800 spectrometer with nonmonochromatic Mg Kα radiation at 1253.6 eV (144 W, 40 eV pass energy). A take-off angle of 45° was used for XPS damage and measurement. High-resolution XPS scans of regions of interest were acquired after a given number of hours of running survey spectra.

Acknowledgment. This work was supported by NSF-DMR98-75788 and by ONR/DARPA N00014-01-1-0658. The DOE Radiation Lab generously provided access to an atomic force microscope. The instrument used for AFM lithography was supported by NSF ECS99-76577.

LA035291E